Chapter 20
Chirality and Its Application

Hisako Sato and Akihiko Yamagishi

20.1 Introduction

"Molecular recognition" is one of the most extensively studied topics in chemistry. A number of biomimetic systems such as crown ethers, cryptands, and cyclodextrins are designed as artificial sites to activate an appropriate substrate in a specific way. In comparison to the molecular systems in homogenous phases, the surface of a solid provides another possibility for molecular recognition. The clean surface of a metal single crystal, for example, provides information on an atomic scale how a molecule interacts with a surface or with its neighbors. In this chapter, the works on the chiral aspects of smectite clays were reviewed. In comparison to metals or bulk metal oxides, smectite clays are characterized by the following unique features from the view point of molecular recognition: (1) two-dimensional network structures of a phyllosilicate sheet, (2) high cation exchange capacity, and (3) exfoliation into inorganic nanosheets.

In the following, the works on the use of smectite clays for optical resolution, asymmetric syntheses, and electrochemical and photochemical reactions are reviewed. An attention is focused on how the above structural characters contributed to the recognition of molecular chirality on a clay surface.

H. Sato (✉)
Graduate School of Science and Engineering, Ehime University,
2-5, Bunkyo-Cho, Matsuyama 790-8577, Japan
e-mail: sato.hisako.my@ehime-u.ac.jp

A. Yamagishi
Faculty of Medicine, Toho University, 5-21-16, Omori-Nishi,
Ota-Ku, Tokyo 143-8540, Japan

T. Nakato et al. (eds.), *Inorganic Nanosheets and Nanosheet-Based Materials*,
Nanostructure Science and Technology, DOI 10.1007/978-4-431-56496-6_20

20.2 Structural Studies on the Chiral Crystal of Kaolinite

Kaolinite ($Al_4[Si_4O_{10}](OH)_8$) is a 1:1 dioctahedral phyllosilicate (layered aluminosilicate) with little isomorphous substitution. Each layer consists of a sheet of SiO_4 tetrahedra forming six-membered silicate rings connected via a common apical oxygen atom to a sheet of edge-sharing [AlO_6] octahedra. Three polytypes are found in nature: kaolinite, dickite, and nacrite. These minerals are stacked with different positions of octahedral vacancies in successive layers. The crystal structure of kaolinite (non-H atoms) was first reported using powder X-ray diffraction. Bailey demonstrated that both kaolinite and dickite are based on a 1*M* stacking sequence of layers [1]. It has been shown that octahedral site vacancies alternate in dickite, whereas in kaolinite the location of the vacancy is the same in repeating layers. In the 1*M* structure, there are three possible locations of the vacant octahedral site, denoted as A-, B-, or C-site vacancies. If the vacant site occurs at the B- or C-site, the structures are chiral; in the case of the A-vacant site, the structure is achiral. In nature, the vacant site of kaolinite occurs in the C (or B) position resulting in a chiral structure.

The first-principles calculations of kaolinite are performed using density functional theory (DFT) [2]. The lattice parameters and structures of the three 1*M* polytypes of kaolinite (vacancies in the A, B, and C positions) were optimized using the exchange-correlation functional (PBE functional). The cell shape and internal atomic coordinates were systematically optimized to search the minimum of total energy. For such calculation, space group *P1* was used as a reduced cell in order to reduce the number of atoms to half of that for the ordinary cell (*C1*). The optimized structures of kaolinite modeled with A-, B-, and C-site vacancies, using *C1* and *P1* unit cells, respectively, are shown in Fig. 20.1. The calculated values of bond lengths for the C-site polytype are in good agreement with experimental data based on the kaolinite structure. It is interesting to see whether the chiral structure is preferred from the energetic point of view. Comparing the formation energies, the chiral polymorphs of kaolinite (B- or C-site vacancy) have similar formation energies as dickite and nacrite, while achiral kaolinite with A-site vacancy is only slightly less stable than the other polytypes (Table 20.1).

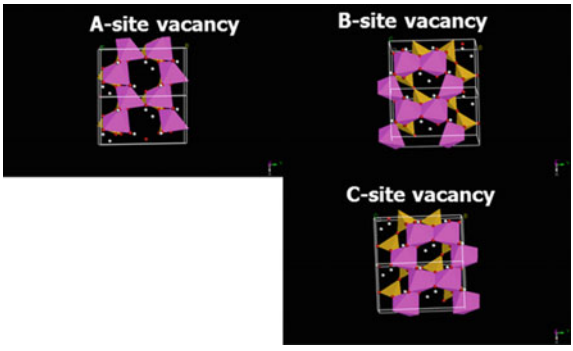

Fig. 20.1 Optimized structures of kaolinite polytypes

Table 20.1 Optimized energy of kaolin polytypes

Polytype	Kaolinite with A-site	Kaolinite with B-site	Kaolinite with C-site
ΔE (kJ/mol)	−1.671	−1.858	−2.050

Note $\Delta E = E–E$(kaolinite single layer)

Kogure and Inoue [3] reported the stacking defect structures in kaolin minerals by applying TEM imaging technique on near-atomic resolution. Electron diffraction and high-resolution imaging of dickite showed that few stacking defects exist in this polytype. On the other hand, kaolinite crystals contain high density of stacking defects. Disorder by the coexistence of B layer and C layer, or dickite-like stacking sequence was never observed. These results provided not only an unambiguous settlement for the long controversy of the defect structures in kaolinite, but also a new clue to understanding kaolinite-to-dickite transformation mechanism. They also reported the chiral structure of a single crystal of kaolinite. By means of back-scattered electron diffraction, it was elucidated that a single crystal of kaolinite itself was chiral [4].

20.3 Stereochemistry Related to the Two-Dimensional Network of a Smectite Clay Surface

There have been extensive efforts to apply a solid surface as a site providing chiral substances on a preparative scale [5, 6]. The finding described in this section opened a possibility of developing such a method on the basis of clay minerals.

20.3.1 Spectroscopic Studies on the Adsorption of Metal Complexes by a Smectite Clay

It was reported that some biological substances such as amino acids and glucoses were adsorbed stereoselectively by natural montmorillonite or vermiculite clay [7–9]. If it was the case, the fact might have profound significance in chiral selection during the period of the chemical evolution. Motivated by the work, the adsorption of chiral molecules was studied by colloidally dispersed sodium montmorillonite. As an adsorbate, tris(1,10-phenanthroline)metal(II) ($[M(phen)_3]^{2+}$) (phen = 1,10-phenanthroline) was chosen [10]. The complex was known to be adsorbed strongly by clay minerals. Moreover, its rigid and highly symmetric properties were expected to be helpful in detecting the subtle difference of adsorption structures between optical antipodes rather than flexible bioorganic molecules.

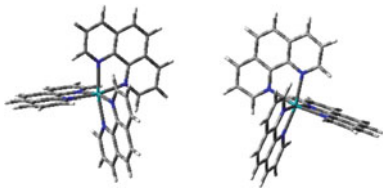

Fig. 20.2 Chiral structures of a tris-chelated metal complex: (*left*) Δ-isomer and (*right*) Λ-isomer

The enantiomers of $[M(phen)_3]^{2+}$ are denoted as Δ- and Λ-isomers, depending on the direction of helical twisting (Fig. 20.2). The adsorption of enantiomeric $[Ru(phen)_3]^{2+}$ by a clay was studied by measuring the electronic absorption spectrum of a colloidal dispersion. When Δ-$[Ru(phen)_3]Cl_2$ was added to an aqueous dispersion of sodium montmorillonite, the metal-to-ligand charge-transfer (MLCT) transition band around 450 nm increased its intensity and shifted toward the longer wavelength with the simultaneous decrease of the π–π* transition band localized in the ligands around 270 nm. These spectroscopic changes were caused by the adsorption of the chelate by a clay particle. No effect of molecular chirality was detected, when the spectral change was compared between the Δ- and Λ-enantiomers of $[Ru(phen)_3]^{2+}$.

When the same experiments were performed for a racemic mixture of $[Ru(phen)_3]^{2+}$, the change of the electronic spectrum was distinctly different from the enantiomeric case. The bathochromic shift of the MLCT transition band was more enhanced and the π–π* transition band split into two composites. In addition to the spectroscopic differences, a remarkable difference was observed in the adsorption amounts. The chelates were adsorbed so strongly that the amount of adsorption increased linearly with the increase of an added clay amount. In case of the enantiomer, the adsorption was saturated when the ratio of clay-to-metal chelate (denoted as [clay]/[chelate]) attained the value of 2, where [clay] and [chelate] were measured in terms of the CEC equivalent/L and mole/L, respectively. The results were reasonable since $[Ru(phen)_3]^{2+}$ carried two positive charges and neutralized two negative charges on adsorption by a clay. Contrary to this, in case of the racemic mixture, the adsorption was saturated already at [clay]/[chelate] = 1. In other words, the chelate was adsorbed to two times excess over the CEC, including external anions for electric neutrality.

The above facts indicated that the chelates interacted with each other on a clay surface in a stereoselective way. Here "stereoselective way" means that the situations are different whether the interacting two molecules are a Δ–Δ (or Λ–Λ) pair or a Δ–Λ pair. If the interaction was indifferent to such chirality effects, no difference would have appeared whether the chelates were added as a pure enantiomer or as a racemic mixture. The fact that the racemic mixture was adsorbed to two times excess of the enantiomers suggested that the chelates preferred to form a racemic pair on a clay surface. This type of adsorption is denoted as "racemic adsorption by clays."

The adsorption by sodium montmorillonite was investigated over the wide range of chiral chelates [11–13]. Table 20.2 lists the classification of investigated chelates

Table 20.2 Classification of metal chelates according to the stereochemical effects on adsorption by a clay

Chelates showing racemic adsorption
$[M(phen)_3]^{2+}$ (M = Ni, Fe, Ru and Os) (phen = 1,10-phenanthroline)
$[Fe(phen)_2(CN)_2]$
$[Co(PAN)_2]^{2+}$ (PAN = pyridylazoresorcinol)
$[Co(PAN)_2]^{+}$
Chelates showing enantiomeric adsorption
$[Ru(bpy)_3]^{2+}$ (bpy = 2,2′-bipyridine)
Chelates showing no stereochemical effect
$[Co(phen)_3]^{3+}$
$[Co(en)_3]^{3+}$ (en = ethylenediamine)
cis-$[Co(en)_2Cl_2]^{+}$

according to the stereochemical effects on adsorption behavior. As deduced from the table, the chelate that shows either racemic or enantiomeric adsorption is coordinated with two or three bulky planar ligands and carries an electric charge of less than two. These facts are consistent with a view that the discrimination of chirality of an adsorbed molecule is performed by the stereochemical interaction between the adjacent molecules on a clay surface. Such interaction might be low for metal complexes with small ligands such as ethylenediamine. Electrostatic repulsion is too large to have chelates stacked, if they are too positive like $[Co(phen)_3]^{3+}$.

No stereochemical effect was observed when $[M(phen)_3]^{2+}$ was adsorbed by other ion exchangers such as cation-exchanging resins, zirconium phosphates, and layered niobates. Thus the phenomena are particular to smectite clays. The structural origin of racemic adsorption was investigated by applying a number of spectroscopic methods such as XRD [14], electric dichroism [15], ESR [16], photoelectron spectroscopy [17], and AFM [18] together with the theoretical calculation [19].

When the thin film of an ion-exchange adduct of racemic $[Os(phen)_3]^{2+}$/montmorillonite was analyzed by in-plane XRD measurements, the two-dimensional regularity existed with the periodicity of 0.95 nm [20]. Scanning tunneling microscopy (STM) was successful only for highly crystalline clay minerals like hydrotalcite [21].

The basal spacing (d_{001}) was determined by XRD measurements for the adducts of sodium montmorillonite and $[M(phen)_3]^{2+}$. The value of d_{001} was 1.78 nm when the chelate was adsorbed to the CEC of a clay. Subtracting the thickness of one layer (0.95 nm) from the basal spacing, the height of the interlayer space was estimated to be 0.83 nm. This height was nearly equal to that of $[M(phen)_3]^{2+}$ along its C_3 axis. The basal spacing of a clay–chelate adduct was expanded to 2.90 nm when the chelate was adsorbed to two times excess of CEC. Accordingly the height of the interlayer space was estimated to be 1.95 nm. The Fourier analyses for a sample of a 2:1 adduct of a clay and racemic $[Fe(phen)_3]^{2+}$ showed that the adsorbates formed a double-molecular layer in the interlayer space. The peak of

electron density in the middle of the space was ascribed to the external anion, SO_4^{2-}, which compensated the excess positive charge [14].

Electro-optical measurements were applied to determine the orientation of $[Ru(phen)_3]^{2+}$ bound on the surface of a colloidal clay particle. According to the method, an electric field pulse was applied to a dispersion containing a colloidal clay and the chelate. The anisotropy in optical absorption (dichroism) was induced by the alignment of an exfoliated clay platelet in the direction of electric field. The electric dichroism was monitored by linearly polarized light. The rise and decay of the signals corresponded to the orientation and de-orientation processes of clay particles in the presence and absence of electric field, respectively. The magnitude of the dichroism is related to the angle, θ, between the electric field and the polarization of the monitoring light as below:

$$\Delta A/A = (\rho/6)(1 + 3\ \cos\ 2\theta). \tag{1}$$

At the limit of complete orientation, ρ, the reduced linear dichroism, is expressed by

$$\rho = (-3/8)(1-3\ \cos\ 2\phi) \tag{2}$$

in which ϕ is the angle between the C_3 axis of the chelate and the direction normal to a clay surface. The angle, ϕ, was obtained to be close to zero or the chelate was adsorbed with its C_3 axis perpendicularly to a clay surface as shown in Fig. 20.3.

The adsorption of a cationic metal complex, $[Ru(phen)_3]^{2+}$, onto a mica surface from its aqueous solution was investigated with atomic force microscopy (AFM). An attention was focused on the effect of molecular chirality on the structures of adsorption layers. AFM observation showed that the surface remained smooth when a mica surface was in contact with an aqueous solution of racemic $[Ru(phen)_3](ClO_4)_2$, while the surface was rough in contact with an Δ-enantiomeric solution. The difference was interpreted in terms of the formation of the compact bimolecular layer for the racemic mixture, while a rough multilayer adsorption layer was formed for the enantiomer [22]. The results were interpreted by the assumption that the racemic adsorption layer was composed of the unit of closely packed

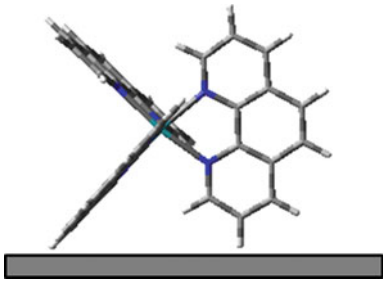

Fig. 20.3 The orientation of $[M(phen)_3]^{2+}$ adsorbed on a smectite clay surface

racemic pairs, while the enantiomeric adsorption layer was composed of two domains or double-molecular and monomolecular layers.

The kinetic formation of the adsorption layer of racemic chelates was studied by means of a stopped-flow electric dichroism apparatus [14]. The rate was compared between the following two cases: (a) a dispersion of a Δ-$[Ru(phen)_3]^{2+}$/clay (denoting a clay particle adsorbing the chelate to CEC) was mixed with a solution of Λ-$[Ru(phen)_3]Cl_2$ and (b) a dispersion of a racemic $[Ru(phen)_3]^{2+}$/clay was mixed with a solution of racemic $[Ru(phen)_3]Cl_2$. For both cases, electric dichroism amplitude ($\Delta A/A$) and absorbance (A) increased on mixing, indicating the occurrence of adsorption in excess over the CEC. The rates of increases were higher for (a) than for (b). The results were rationalized in terms of the mechanism that, in case of (a), the racemic layer was formed simply by pairing a pre-adsorbed Δ-$[Ru(phen)_3]^{2+}$ with an incoming Λ-$[Ru(phen)_3]^{2+}$, while, in case of (b), the process of molecular rearrangement was required among the pre-adsorbed racemic chelates before a racemic pair was formed.

Breu et al. also performed the experiments on the intercalation of metal complexes by a smectite clay. In case of the intercalation compounds of natural smectites, no 2D long-range order of the interlamellar space was observed. To this contrary, the in-plane order was detected using a homogeneously charged synthetic fluorohectorite as a host material. With these intercalates, the distinct 2D structures for enantiopure and racemic $[Ru(bpy)_3]^{2+}$ interlayers as previously predicted by atomistic simulations could be proven experimentally [23].

Villemure [13] reported the absorption of enantiomeric $[Ru(bpy)_3]^{2+}$ by several different kinds of smectite samples. The absorption of racemic mixture was lower than that of pure enantiomer. The enantiomer was absorbed in excess over CEC.

20.3.2 *Theoretical Studies of Racemic Adsorption and Its Significance for Chiral Recognition*

The adsorption behavior was simulated theoretically by use of Monte Carlo technique [19]. The calculation showed the predicted bound states of a pair of racemic and enantiomeric $[M(phen)_3]^{2+}$ molecules at the minimum binding energy, respectively. As was expected, a racemic pair forms an associate with their ligands interlocked closely, while an enantiomeric pair forms a loose associate due to the steric repulsion between the facing ligands. When the free energy was calculated statistically using a Metropolis algorism, the racemic and enantiomeric pairs took the sharp minima of free energy at the intermolecular distances of 0.95 and 1.42 nm, respectively. One important deduction of the above model is that there exists a vacant space surrounded by the bound chelates when a clay surface is covered with enantiomeric $[M(phen)_3]^{2+}$. Such a space is stereoselective toward further adsorption, since it accepts exclusively its optical antipode. Based on this hypothesis, an ion-exchange adduct of enantiomeric $[M(phen)_3]^{2+}$ (M = Ni,

Ru)/clay was used as a chiral adsorbent for optical resolution and asymmetric syntheses. A number of examples have been accumulated to demonstrate the capability of such a surface in discriminating molecular chirality.

Breu et al. also simulated the metal complexes on a clay surface. Lattice energy minimization techniques were used to study the 2D molecular organization of $[Ru(bpy)_3]^{2+}$ and $[Ru(phen)_3]^{2+}$ confined in the interlamellar space of low-charged smectites. With racemic pillars, favorable π stacking lead to the clustering of pillars even with homogeneously charged smectites. Long-range and/or short-range ordering of the isomorphous substitution within the silicate layer strongly influence the interlayer structure, since host–guest interactions are dominated by electrostatics [24].

20.4 Chirality Recognition by a Clay Modified with Metal Complexes

20.4.1 Anti-racemization of Labile Metal Complexes

One example was shown to show how chirality was recognized by the adsorbed molecules on the surface of a smectite clay [25]. A labile complex, $[Fe(phen)_3]^{2+}$, racemizes with a half-life time ($t_{1/2}$) of 25 min in water at 25 °C, while $[Ni(phen)_3]^{2+}$ is less labile with $t_{1/2}$ = 3 h under the same conditions. Racemic $[Fe(phen)_3]Cl_2$ was added to an aqueous dispersion of a Δ-$[Ni(phen)_3]^{2+}$/clay. The amount of added $[Fe(phen)_3]^{2+}$ was below the CEC. When the dispersion was monitored by the circular dichroism (CD) spectrum, no CD activity was observed initially in the wavelength region of 350–700 nm. This was because Δ-$[Ni(phen)_3]^{2+}$ was nearly transparent in this wavelength region. The CD band appeared in several minutes and developed in hours until it nearly coincided with the CD spectrum of Λ-$[Fe(phen)_3]^{2+}$. The results were rationalized in terms of the mechanism: (i) Λ-$[Fe(phen)_3]^{2+}$, half of added $[Fe(phen)_3]^{2+}$, was adsorbed instantly by a Δ-$[Ni(phen)_3]^{2+}$/clay; (ii) the remaining Δ-$[Fe(phen)_3]^{2+}$ racemized gradually in water to Λ-$[Fe(phen)_3]^{2+}$ and was adsorbed by a Δ-$[Ni(phen)_3]^{2+}$/clay; and finally (iii) the whole of added $[Fe(phen)_3]^{2+}$ ions was stabilized as the Λ-form by pairing with Δ-$[Ni(phen)_3]^{2+}$ on a smectite clay surface.

20.4.2 Clay Column Chromatography for Optical Resolution

The chiral recognition by the modified surface of a smectite clay lead to the development of chromatographic resolution [26, 27]. A spherically shaped aggregate was prepared by spray drying an aqueous dispersion of synthetic hetorite.

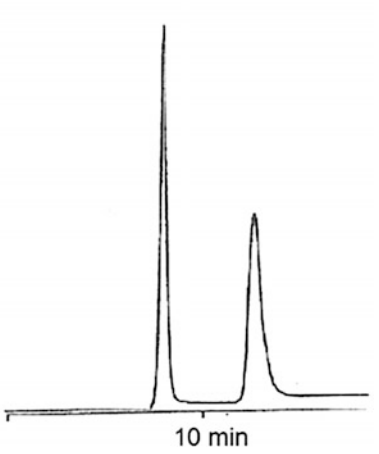

Fig. 20.4 The chromatogram when a racemic mixture of 1,1′-bi-2-naphthol was eluted on a column packed with Λ-$[Ru(phen)_3]^{2+}$/synthetic hectorite with methanol. The *first* and *second peaks* are *R*- and *S*-enantiomers, respectively

Particles of a size of c.a. 5 μm were soaked in a methanol solution containing Λ-$[Ru(phen)_3]Cl_2$. The ion exchanging of Λ-$[Ru(phen)_3]^{2+}$ into a clay took place in seconds to produce a yellow-colored solid. The material was packed into a stainless steel tube and used as a column for high-performance liquid chromatography (HPLC) [28, 29].

Figure 20.4 shows the chromatogram when a racemic mixture of 1,1′-bi-2-naphthol was eluted on the column (4 mm (i.d.) × 250 mm) with methanol. Two peaks with the equal area were obtained on the base-line separation. From the CD spectra, the less and more retaining peaks contained the pure *R*- and *S*-enantiomers of 1,1′-bi-2-naphthol, respectively. The separation factor was calculated to be 1.78, which was quite large in comparison to the known chiral columns. The enthalpy change ($-\Delta H$) of adsorption was determined from the temperature dependence of the retention times: $-\Delta H$ = 3.1 and 5.7 kJ mol^{-1} for the *R*- and *S*-1,1′-bi-2-naphthol, respectively. Thus the high separation capability of the present column was ascribed to the large difference of adsorption enthalpy (∼2.6 kJ mol^{-1}). From the XRD measurements, the basal spacings of ternary adducts of a clay, Δ-$[Ru(phen)_3]^{2+}$ and *R*- or *S*-1,1′-bi-2-naphthol was obtained to be 2.78 or 2.45 nm, respectively. The more strongly adsorbed *S*-enantiomer gave the narrower spacing, or it was located closer to a clay surface, probably forming a side-by-side associate with Λ-$[Ru(phen)_3]$.

The clay column exhibited the following characteristics from the practical point of view:

1. Performance is stable and reproducible for a long time against the change of temperature or eluting solvents (except for water).
2. Resolution capacity is high (e.g., 400 mg of $[Ru(acac)_3]$ was resolved for a single run on a 20 mm (i.d.) × 250 mm column).

3. Antipodal columns, or Δ-$[Ru(phen)_3]^{2+}$/clay and Λ-$[Ru(phen)_3]^{2+}$/clay are both available. This is particularly useful in separating a mixture of diastereomeric species [30].
4. The systematic modification of a packing material is possible to tune resolution capability by changing the structure of a pre-adsorbed chelate (e.g., $[Ru(bpy)_3]^{2+}$/clay) [25].

A column packed with Δ-$[Ru(phen)_3]^{2+}$/synthetic hectorite is commercially available and is used for separating wide range of organic and inorganic compounds [Ceramosphere Ru-1, Shiseido (Japan)]. As one of the recent applications, all of the four diastereomers of a star-burst type tetranuclear ruthenium(III) complex was resolved. The diastereomers were differentiated by the parts connecting the core and periphery regions. Thus the column discriminated local chirality within a large molecule [31, 32].

20.4.3 Photochemistry on a Modified Surface

Asymmetric catalysis driven by visible light is regarded as one of the most promising environmentally friendly methods [33]. One promising attempt to enhance chiral selectivity is the immobilization of a chiral catalyst onto a solid surface [34]. Such heterogeneous photochemistry has been explored using organic and inorganic hosts. For practical uses, the immobilization of a chiral species in a solid leads to an advantage of the versatile separation of a catalyst from a solution as well as the avoiding of effluxes of poisonous metals. Only a few heterogeneous asymmetric catalysis has been reported in photochemistry probably because of the difficulties in the preparations of suitable solid supports [35]. In the following, the photochemical reactions of clay minerals have been reviewed by Shichi and Takagi [36].

20.4.3.1 Asymmetric Syntheses

The ion-exchange adducts of a clay and a metal chelate was utilized as an adsorbent to produce chiral molecules. Figure 20.5 shows the basic principle for it. A prochiral molecule is adsorbed on a void space surrounded by chiral chelates. When the bound molecule undergoes a chemical change, it might transform to an optically active molecule under the steric control of the surrounding chelates.

As an example, phenyl alkyl sulfide was adsorbed by an adduct of sodium montmorillonite ion exchanged with either chiral $[Ru(phen)_3]^{2+}$ or $[Ru(bpy)_3]^{2+}$. The adsorbed sulfide was photooxidized to a sulfoxide under the illumination of visible right. The reaction was driven by the photosensitizing action by Ru(II) complexes. The sulfoxide was produced in the chiral form at the enantioselectivity (e. e.) of about 43% [37]. The observed stereoselectivity was ascribed to the

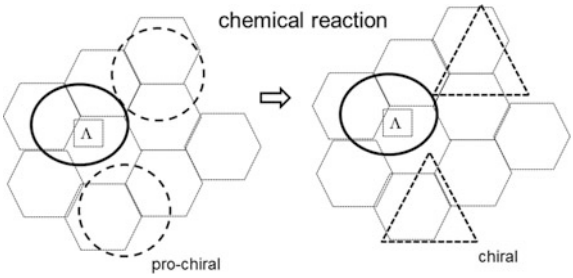

Fig. 20.5 A schematic model for the transformation of a prochiral molecule to chiral one under the steric control of chelates bound on the surface of a smectite clay

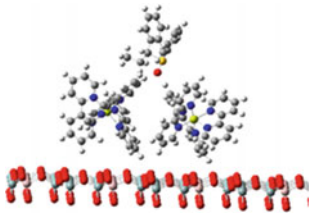

Fig. 20.6 Schematic drawing of the possible reaction paths on a clay surface

selection of reaction paths on a clay surface as shown in Fig. 20.6. The chirality of a sulfoxide molecule was determined under the steric control by pre-adsorbed Ru(II) complexes. It was noted that no chiral induction was attained for the homogenous system (water/methanol medium), even if the same chiral chelates were used as a photosensitizer. Thus the fixation of a substrate on the surface of a smectite clay was essential to chiral recognition.

The above method was applied to the auto-catalytic systems [38]. A prochiral aldehyde was transformed to chiral pyrimidyl alkanol by the catalytic reaction of i-Pr_2Zn. The reaction was performed in the presence of Δ-$[Ru(phen)_3]^{2+}$/clay or Λ-$[Ru(phen)_3]^{2+}$/clay. The enantiomer excess of the product attained as high as 80–90%. Again chiral selectivity was determined by the absolute configuration of the adsorbed chelates.

20.4.3.2 Chiral Ru(II) Metal Complexes on a Clay Surface

Thomas et al. reported the studies on the photophysical processes of tris(2,2′ bipyridine)ruthenium(II) ($[Ru(bpy)_3]^{2+}$) bound to colloidal kaolinite and montmorillonite particles [39–41]. The absorption and emission spectroscopy at room temperature and 77 K were found to be effective in probing the environmental difference between the external surface and internal layers of these minerals. The significant quenching of $[Ru(bpy)_3]^{2+}$ was observed on a montmorillonite containing 4% iron. Hydrazine was used to reduce Fe(III) to Fe(II) in a lattice. This conversion resulted in the decrease in the quenching effect of $[Ru(bpy)_3]^{2+}$. The rate data of fluorescence quenching showed that both cationic and uncharged molecules moved quite freely on a clay surface.

Ghosh and Bard [42, 43] reported the spontaneous racemic and pseudo-racemic interactions between optically active poly(pyridyl) metal chelates ($[Ru(bpy)_3]^{2+}$) which were adsorbed on a smectite clay. The results highlighted differences in the binding modes of these two forms at low loading levels (1–4%). The optical purity, loading level, mode of addition of the complex, and the type of clay minerals had an effect on the observed differences in binding states. Their results revealed that the absorption spectra of an enantiomer and a racemate were different even at low loading and that the spectrum of the latter was understood in terms of two effects: clay–chelate and spontaneous antipode–antipode (or racemic) interactions. These effects were additive for the metal-to-ligand charge-transfer (MLCT) transition. The adsorption of pure enantiomers raised the energy of the emission maximum, while racemic interactions produced a bathochromic shift. The contrasting nature of the absorption (MLCT) and emission trends was rationalized in terms of the assumption that the observed shifts in peak positions were exclusively due to perturbations in the energies of ligand-centered orbital.

Kamat et al. [44] studied the photophysical behavior of enantiomeric and racemic $[Ru(bpy)_3]^{2+}$ on a layered clay. The decrease in the luminescence yield of a racemate on increasing the loading was mainly associated with an attenuation in the peak emission intensity as found from time-resolved measurements. The intensity of luminescence differed nearly two times between enantiomeric and racemic $[Ru(bpy)_3]^{2+}$ even at the low loading level. Besides there existed a definite difference in the peak position of luminescence between the racemic (605 nm) and enantiomeric (586 nm) $[Ru(bpy)_3]^{2+}$. The emission of the racemate falls off rapidly with increased loading from 0 to 50%, whereas the emission from the enantiomeric adsorbate remained almost constant. These results were rationalized in terms of a model that the racemates were clustered locally while the enantiomeric ions were more randomly distributed on a clay surface.

The orientation of a metal complex was tuned by attaching alkyl chains at the different positions of a bpy ligand [45]. It was shown that the orientation of adsorbed polypyridyl Ru(II) complexes ($[Ru(bpy)_2X]^{2+}$ with X = 2,2′-bipyridine, 4,4′-diundecyl-2,2′-bipyridine, and 5,5′-diundecyl-2,2′-bipyridine) had a decisive effect on their chiral discrimination in an energy transfer reaction. The quenching rate of phosphorescence due to an adsorbed Ru(II) chelate was measured for the energy transfer between excited polypyridyl Ru(II) complexes and chiral $[Ru(acac)_3]$ (acac = acetylacetonato). As a results, at the loading of 10% of cation exchange capacity (CEC), the quenching rate constant was nearly equal between the Δ- and Λ-enantiomers of $[Ru(acac)_3]$ within the experimental error (c.a. 5%). Thus no stereoselectivity appeared at this loading level for all three complexes. At the loading of 40% of CEC, however, there was a distinctive difference between the enantiomer of the quencher for all three kinds of Ru(II) chelates. In other words, Δ-$[Ru(acac)_3]$ is more effective than Λ-$[Ru(acac)_3]$ in quenching excited Λ-$[Ru(bpy)_2X]^{2+}$ on a clay surface. Notably such stereoselective effect was largest for the case of $[Ru(bpy)_2$(5,5′-diundecyl-2,2′-bipyridine)$]^{2+}$.

20.4.3.3 Ir(III) Complexes Applied as a Luminescent Modifier on a Clay Surface

Iridium(III) complexes are known to be strongly emissive under the irradiation of visible light. This property was used to prepare photoreactive clay hybrid materials [46–49]. In addition to the emitting properties, some chelated iridium(III) complexes are chiral and stable against racemization at higher temperature. The optical resolution of a cationic iridium(III) complex, $[Ir(ppy)_2dmbpy]^+$ (ppy = 2-phenylpyridine and dmbpy = 4,4′-dimethyl-2,2′-bipyridine), was achieved by means of liquid chromatography on a chiral column [48].

The quenching of excited $[Ir(ppy)_2dmbpy]^+$ (denoted as Ir(III)) was studied in an aqueous dispersion of synthetic saponite [48]. Chiral $[Ru(acac)_3]$ was used as a quencher. The emission intensity at 650 nm was compared between the following two pairs, clay/Δ-Ir(III)/Δ-$[Ru(acac)_3]$ (pseudo-enantiomeric combination) and clay/Δ-Ir(III)/Λ-$[Ru(acac)_3]$ (pseudo-racemic combination), in 3:1 (v/v) water–methanol. In both cases, the intensity of emission decreased on adding $[Ru(acac)_3]$, indicating that Ru(III) complex acted as an efficient quencher. The quenching effect was analyzed in terms of the Stern–Volmer plots. It was revealed that luminescence quenching was more efficient for the clay/Δ-Ir(III)/Δ-$[Ru(acac)_3]$ system than for the clay/Δ-Ir(III)/Λ-$[Ru(acac)_3]$. From the analyses of the plots, the rate of quenching was much higher than the diffusion processes. Therefore, it was suggested that the quenching reaction was not a simple collisional process, but it might involve the process of molecular association on a clay surface. Notably, no stereoselectivity was detected in methanol for the same emitter/quencher pairs. Thus the fixation of the iridium(III) complex on a clay surface was concluded to be a crucial step for chiral recognition.

Sato et al. [49] investigated the energy transfer between two types of iridium(III) complexes, $[Ir(dfppy)_2(C_n\text{-bpy})]^+$ (dfppyH = 2-(2′,4′-difluorophenyl)pyridine; C_n-bpy = 4,4′-dialkyl-2,2′-bipyridine; dialkyl = dimethyl (C_1), didodecyl (C_{12}), and dinonyldecyl (C_{19})) and $[Ir(piq)_2(C_n\text{-bpy})]^+$ (piqH = 1-phenyisoquinoline) as a donor and an acceptor, respectively (Fig. 20.7). The complexes were co-adsorbed by colloidally dispersed synthetic saponite. The efficiency of energy transfer (η_{ET}) was obtained from the emission spectra at various donor-to-acceptor ratios (D/A). The results were analyzed on the basis of the Förster-type energy transfer mechanism. For C_1-bpy, η_{ET} was as high as 0.5 with a D/A of ca. 20. The results implied

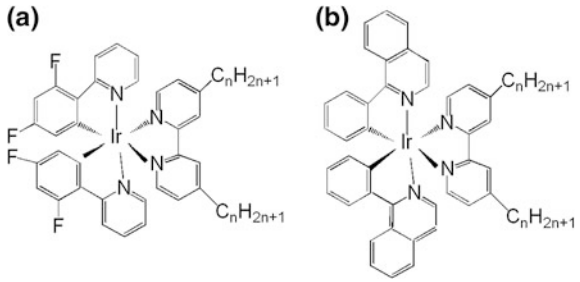

Fig. 20.7 Structures of the Ir(III) complexes, Δ-$[Ir(dfppy)_2(C_n\text{-bpy})]^+$ (dfppyH = 2-(4′,6′-difluorophenyl)pyridine; C_n-bpy = 4,4′-dialkyl-2,2′-bipyridine) (donor) (**a**) and Δ-$[Ir(piq)_2(C_n\text{-bpy})]^+$ (piqH = 1-phenyisoquinoline) (acceptor) (**b**)

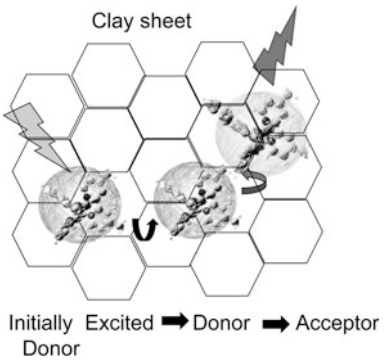

Fig. 20.8 Light-harvesting model on a clay surface

that the photon energy captured by several donor molecules was collected by a single acceptor molecule (i.e., the harvesting of light energy). The harvesting of light energy was considered to occur on a clay surface according to the mechanism as shown in Fig. 20.8. Enantioselectivity was observed in the present type of energy transfer of C_1-bpy, which indicated the participation of a contact pair of donor and acceptor molecules. For C_{12}-bpy and C_{19}-bpy, η_{ET} was low and exhibited no enantioselectivity, because their long alkyl chains inhibited close contact between the donor and acceptor molecules.

20.4.4 Construction of Clay Nano-Sheet Films for Gas Sensing

The Langmuir–Blodgett method preparing a single-layered clay film (denoted as clay-LB) was first reported by two groups (Yamagishi et al. and Kotov et al.) in 1994 [50, 51]. Yamagishi et al. extended their study to the photophysical application of the multilayer films [52]. For preparing a clay-LB film, cationic amphiphiles such as alkylammonium in chloroform was spread over the surface of an aqueous suspension of a clay mineral. Photoreactive metal complexes are replaced with alkylammonium ions simply by immersing a prepared electrode in their aqueous or methanol solution. This is the combination of the Langmuir–Blodgett (LB) method and self-assembly (SA).

The photophysical studies on a clay-modified electrode revealed that a single clay layer acted as an efficient barrier for the occurrence of electron transfer from an amphiphilic polypyridyl Ru(II) complex (electron donor) to an amphiphilic acetylacetonato-Ru(III) complex (electron acceptor). Multi-layered films were prepared, in which an emitter/clay and a quencher/clay were deposited in an alternative way. In such a film, it was revealed that a single clay layer acted as a barrier for the transfer of photon energy [53].

Recently luminescent films have been applied for chemo- and bio-sensing [54–56]. A hybrid film of a clay and iridium(III) complex as described in the previous section was applied for the oxygen sensing [57–60].

20.4.5 Chiral Sensing on an Electrode Modified with a Thin Film of Clay/Chelate Hybrid

The sensing of molecular chirality through the reaction of electron transfer was attempted by use of clay-modified electrodes as described above [61, 62]. As one example, an ITO electrode was modified with a thin film of $[Os(phen)_3]^{2+}$/clay. UV light was irradiated on such an electrode. When Λ-$[Os(phen)_3]^{2+}$/clay was used, the oxidation photocurrent was enhanced in the presence of *R*- (or *S*-1,1′-bi-2-naphthol) in an electrolyte solution. The results indicated that Os(II) complex acted as a mediator catalyzing the oxidation of binaphthol. Notably, the catalytic current was higher for *S*-1,1′-bi-2-naphthol than for *R*-1,1′-bi-2-naphthol by about 1.8 times at 700 mV. This provides a possibility of electrochemical sensing of a chiral molecule.

The current increases linearly with the increase of the concentration up to 0.11 mM of 1,1′-2-binaphthol. Λ-$[Os(phen)_3]^{3+}$ was first generated by photoinduced electron transfer from photoexcited Λ-$[Os(phen)_3]^{2+}$. The oxidized Λ-$[Os(phen)_3]^{3+}$ was reduced to Λ-$[Os(phen)_3]^{2+}$ by 1,1'-2-binaphthol. Stereoselectivity arose from the difference of adsorption strength of the substrate toward a clay surface modified with Λ-$[Os(phen)_3]^{2+}$ complexes. Photocurrent was also measured for other kinds of binaphthyl derivatives. As a result, chiral sensing was successful in case of 1,1′-2-binaphthol and 1,1′-2-binaphthyl amine. These compounds were possible to be oxidized by Λ-$[Os(phen)_3]^{3+}$. Other compounds were not detected because they were resistant to oxidation under the mediating action of adsorbed Os (II) complexes. Thus it was concluded that the present chiral electrode was applicable by the action of oxidation mediator by a photo-responsive molecule adsorbed on an electrode surface.

20.5 Summary and Future Development

Smectite clays were used as an adsorbent for molecular recognition. The surface of a clay was modified with chiral metal complexes. In case of using an enantiopure molecule, either Δ- or Λ-$[Ru(phen)_3]^{2+}$, a microscopic vacant space was generated on such a surface. The space acted as a binding site with stereoselectivity. Since clay minerals are ubiquitous and friendly to the environment, the present method sheds a light on the utility of such a material for the finely controlled chemical reactions.

As for the future development of the present approach, the following possibilities are proposed:

1. To pursue a possibility of obtaining a chiral single crystal of kaolinite [4]. Such an attempt has a significance in both fundamental (as a possible role in generating chiral molecules during the chemical evolution) and practical fields (as a material for chiral support for heterogeneous asymmetric syntheses)
2. To improve the clay column chromatography by selecting metal complexes as a chiral modifier [63]. One target might be to resolve directly non-derivatized aliphatic compounds like amino acids with no aromatic group.
3. To construct a single-layered film of clay nanosheets with high quality. Such a film might be used as an electronic device such as an insulating film with high dielectric constant [64, 65].
4. To manipulate the molecular aggregate on a clay film in which several components such as donor, mediator, and acceptor are arranged in an organized order [49, 59, 66]. Such a system might present an inorganic model for light harvesting in biological photosyntheses.

References

1. Bailey SW (1988) Polytypism of 1:1 layer silicates, Chap. 2 In: Bailey SW(ed) Hydrous phyllosilicates (exclusive of mica). Reviews in mineralogy, vol 19. Mineralogical Society of America, Washington, D.C., pp 9–27
2. Sato H, Ono K, Johnston CT, Yamagishi A (2004) Am Mineral 89:1581–1585
3. Kogure T, Inoue A (2005) Am Mineral 90:85–89
4. Kameda J, Yamagishi A, Kogure T (2005) Am Mineral 90:1462–1465
5. Mallouk TE, Gavin JA (1998) Acc Chem Res 31:209–217
6. Yamagishi A, Sato H (2012) Clays Clay Miner 60:411–419
7. Bondy SC, Harrington M (1979) Science 203:1243–1244
8. Fraser DG, Greenwell HC, Skipper NT, Smalley MV, Wilkinson MV, Demé B, Heenan RK (2011) Phys Chem Chem Phys 13:825–830
9. Fraser DG, Fitz D, Jakschitz T, Rode BM (2011) Phys Chem Chem Phys 13:831–838
10. Yamagishi A, Soma M (1981) J Am Chem Soc 103:4640–4642
11. Yamagishi A (1982) J Phys Chem 86:2474–2479
12. Yamagishi A, Fujita N (1984) J Colloidal Interface Sci 100:136–142
13. Villemure G (1990) Clays Clay Miner 38:622–630
14. Taniguchi M, Yamagishi A, Iwamoto T (1991) J Phys Chem 30:2462–2467
15. Yamagishi A, Taniguchi M, Takahashi M, Asada C, Matsushita N, Sato H (1994) J Phys Chem 98:7555–7561
16. Yano Y, Watanabe T, Taniguchi M, Yamagishi A (1992) Clay Sci 8:381–391
17. Yamagishi A, Tanaka K, Toyoshima I (1982) Chem Commun 343–345
18. Takahashi S, Tanaka R, Wakabayashi N, Taniguchi M, Yamagishi A (2003) Langmuir 19:6122–6125
19. Sato H, Yamagishi A, Kato S (1992) J Am Chem Soc 114:10933–10940
20. Umemura Y, Shinohara E (2004) Chem Commun 42:1110–1111
21. Yao Y, Taniguchi M, Nakata M, Takahashi M, Yamagishi A (1998) Langmuir 14:2890–2895

22. Wakabayashi N, Nishimura SI, Kakegawa N, Sato H, Yamagishi A (2004) Clay Sci 12:259–266
23. Breu J, Stoll A, Lange KG, Probst T (2001) Phys Chem Chem Phys 3:1232–1235
24. Breu J, Nilesh RN, Catlow CRA (1999) J Chem Soc Dalton Trans 835–845
25. Yamagishi A (1985) Inorg Chem 24:1689–1695
26. Yamagishi A (1985) J Am Chem Soc 107:732–733
27. Yamagishi A, Taniguchi M, Imamura Y, Sato H (1996) Appl Clay Sci 11:1–10
28. Nakamura Y, Yamagishi A, Matsumoto A, Tohkubo K, Ohtsu Y (1988) J Chromatogr 482:165–167
29. Kakegawa N, Yamagishi A (2005) Chem Mater 17:2997–3003
30. Sato H, Mori Y, Fukuda Y, Yamagishi A (2009) Inorg Chem 48:4353–4361
31. Fujimoto N, Mori Y, Yamagishi A, Sato H (2010) Chem Commun 46:5473–5474
32. Sato H, Sato F, Taniguchi M, Yamagishi A (2012) Dalton Trans 41:1709–1712
33. Huo H, Shen X, Wang C, Zhang L, Röse P, Chen LA, Harms K, Marsch M, Hilt G, Meggers E (2014) Nature 515:100–103
34. Yamagishi A (1987) J Coord Chem 16:131–211
35. Sato H, Yamagishi A (2007) J Photochem Photobiol, C 8:67–84
36. Shichi T, Takagi K (2000) J Photochem Photobiol, C 1:113–130
37. Fujita S, Sato H, Kakegawa N, Yamagishi A (2006) J Phys Chem B 110:2533–2540
38. Kawasaki T, Omine T, Suzuki K, Sato H, Yamagishi A, Soai K (2009) Org Biomol Chem 7:1073–1075
39. Thomas JK (1988) Acc Chem Res 21:275–280
40. Dellaguardia RA, Thomas JK (1983) J Phys Chem 87:990–998
41. Chu DY, Thomas JK (1985) J Phys Chem 89:4065–4070
42. Ghosh PK, Bard AJ (1984) J Phys Chem 88:5519–5526
43. Ghosh PK, Bard AJ (1983) J Am Chem Soc 105:5691–5693
44. Kamat PV, Gopidas KR, Mukherjee T, Joshi V, Kotkar D, Pathak VS, Ghosh PK (1991) J Phys Chem 95:10009–10018
45. Sato H, Hiroe Y, Tamura K, Yamagishi A (2005) J Phys Chem B 109:18935–18941
46. Sato H, Tamura K, Taniguchi M, Yamagishi A (2009) Chem Lett 38:14–15
47. Sato H, Tamura K, Taniguchi M, Yamagishi A (2014) Appl Clay Sci 97–98:84–90
48. Sato H, Tamura K, Aoki R, Kato M, Yamagishi A (2011) Chem Lett 40:65–67
49. Tamura K, Yamagishi A, Kitazawa T, Sato H (2015) Phys Chem Chem Phys 17:18288–18293
50. Inukai K, Hotta Y, Taniguchi M, Tomura S, Yamagishi A (1994) J Chem Soc Chem Commun 959–960
51. Kotov NA, Meldrum FC, Fendler JH, Tombacz E, Dekany I (1994) Langmuir 10:3797–3804
52. Tamura K, Setsuda H, Taniguchi M, Yamagishi A (1999) Langmuir 15:6915–6920
53. Inukai K, Hotta Y, Tomura S, Takahashi M, Yamagishi A (2000) Langmuir 16:7679–7684
54. Umemura Y, Koura A, Nishioka T, Tanaka D, Shinohara E, Suzuki T, Sasaki T (2010) J Phys Chem C 114:19697–19703
55. Guan W, Zhou W, Lu J, Lu C (2015) Chem Soc Rev 44:6981–7009
56. Sato H, Tamura K, Taniguchi M, Yamagishi A (2010) New J Chem 34:617–622
57. Sato H, Tamura K, Ohara K, Nagaoka S, Yamagishi A (2011) New J Chem 35:394–399
58. Morimoto K, Nakae T, Ohara K, Tamura K, Nagaoka S, Sato H (2012) New J Chem 36:2467–2471
59. Sato H, Tamura K, Ohara K, Nagaoka S (2014) New J Chem 38:132–138
60. Sato H, Ochi M, Kato M, Tamura K, Yamagishi A (2014) New J Chem 38:5715–5720
61. He J, Sato H, Umemura Y, Yamagishi A (2005) J Phys Chem B 109:4679–4683
62. Yoshida J, Saruwatari K, Kameda J, Sato H, Yamagishi A, Sun L, Corriea M, Villemure G (2006) Langmuir 22:9591–9597
63. Okada T, Kumasaki A, Shimizu K, Yamagishi A, Sato H (2016) J Chromatogr Sci 54: 1238–1243

64. Sato H, Okamoto K, Tamura K, Yamada H, Saruwatari K, Kogure T, Yamagishi A (2008) Appl Phys Expr 1:035001–035003
65. Kim SS, Khai TV, Kulish V, Kim Y-H, Na HG, Katoch A, Osada M, Wu P, Kim HW (2015) Chem Mater 27:4222–4228
66. Ohtani Y, Nishinaka H, Hoshino S, Shimada T, Takagi S (2015) J Photochem Photobiol, A 313:15–18